Enhanced single-ion conduction and free-standing properties of solid polymer electrolyte by incorporating a polyelectrolyte

Materials Research Express

PAPER

Enhanced single-ion conduction and free-standing properties of solid polymer electrolyte by incorporating a polyelectrolyte

Tewuhibo S Mengistie[1,2], **Jang Myoun Ko**[1] **and Jung Yong Kim**[2,3]

[1] Department of Chemical and Biological Engineering, Hanbat National University, Daejeon 34158, Republic of Korea
[2] School of Materials Science and Engineering, Jimma Institute of Technology, Jimma University, PO Box 378, Jimma, Ethiopia
[3] School of Chemical Engineering, Jimma Institute of Technology, Jimma University, PO Box 378, Jimma, Ethiopia

E-mail: jungyong.kim@ju.edu.et

Keywords: ionic conductivity, polyelectrolyte, single ion conductor, solid polymer electrolyte, Vogel-Tammann-Fulcher (VTF) equation, free standing property, Li-ion transference number

OPEN ACCESS

RECEIVED
8 February 2021

REVISED
8 March 2021

ACCEPTED FOR PUBLICATION
11 March 2021

PUBLISHED
24 March 2021

Abstract

A free-standing solid polymer electrolyte (SPE) composed of poly(ethylene oxide) (PEO), bis (trifluoromethanesulfonyl)imide (LiTFSI), and poly(lithium 4-styrenesulfonate) (PLSS) was developed in this work. Thermal analysis indicated that the melting points of PEO were depressed with increasing the salt additives, LiTFSI and PLSS. At the composition of [EO]:LiTFSI:[LSS] = 14:1:1, the SPE exhibited a crystallinity of 7.75%, and a crystallite size of 30.62 nm on the (120) crystallographic plane. [EO] and [LSS] represent the structural unit of PEO and PLSS, respectively. This SPE also exhibited an ionic conductivity (σ) of 1.70×10^{-5} S cm^{-1} at 25 °C and 1.04×10^{-4} S cm^{-1} at 45 °C. For analyzing the temperature dependence of σ, the Vogel-Tammann-Fulcher equation was employed. Resultantly, a pseudo activation energy (E_a = 0.1552 eV), a prefactor (A = 206.0338 S cm^{-1} K$^{1/2}$), and an empirical constant (B = 1800.5879 K) were obtained using the optimized [EO]:[Li$^+$] = 7:1 complex. The SPE showed an electrochemical stability window of ~4.7 ± 0.1 V versus Li/Li$^+$. Through DC polarization and AC impedance, the Li-ion transference number of 0.66 was obtained at 70 °C. Finally, when a Li/SPE/$LiFePO_4$ cell was prepared, the device exhibited a discharge capacity of 121 mAh g^{-1} at 50 °C with a coulombic efficiency close to 100%.

Introduction

Li–ion batteries (LIBs) have been the most commercially successful primary power source for portable electronic devices due to their high energy density, low rate of self-discharge, low weight and zero memory effect [1–3]. Their applications have also extended to electric vehicles and various grid–scale energy storage applications [4–7]. However, LIBs have various limitations including safety problems related with liquid electrolytes [8–11]. Hence, attempts have been made to replace this liquid electrolyte with a solid polymer electrolyte (SPE) to solve this leakage problem. The origin of SPE could be ascribed to the fundamental observation that there is an ionic nature in poly(ethylene oxide) (PEO)-salt complexes [12]. It was suggested that such complexes could be used as a solid electrolyte for electrochemical devices [13]. Since then, there have been tremendous research efforts to develop SPEs for thin and safe LIBs and supercapacitors [14]. SPEs have many practical advantages such as minimized dendritic formation, design flexibility, high voltage usage, low cost fabrication, and size scalability, which are desirable for the safe operation of energy storage devices.

SPEs can serve not only as an ionic charge transport layer, but also as a separator between two electrodes, e.g. the cathode and anode. For these functions, SPEs need a polymer as a solid solvent with a Lewis base moiety (e.g. oxygen atoms in the structural unit of PEO) allowing a coordinated bonding with Li–cations. Also SPEs undergo a volume change during charge/discharge cycles by accommodating ions. To date, in the field of SPEs, PEO has been the benchmark solvating polymer with lone–pair electrons on ether oxygen, which has the material properties of density (ρ = ~1.20–1.22 g cm^{-3}), dielectric constant ($\varepsilon_r \approx 5$), crystallinity (χ_c = ~70%–80%), 7/2 helix (7 repeat units with 2 turns, leading to ~1.93 nm), C–O bond's low torsional barrier (6.3 kJ/mol),

melting point (T_m = ~65–71 °C), glass transitional temperature ($T_g \approx -60$ °C), and monoclinic lattice with unit cell parameters (**a** = 0.805 nm, **b** = 1.304 nm, **c** = 1.948 nm, and angle = 125.4°) [13, 15–19]. For effective ethylene oxide-cation interactions and complexations (i.e. to form solid solutions), the bulky anion with a small lattice energy is usually required [20]. In the PEO–salt complexes [21], the ionic charge transport mechanism has been an interesting topic. Some researchers reported that a PEO–LiX (X = PF_6, AsF_6, SbF_6) crystalline complex has a fast Li–ion migration through a cylindrical tunnel formed by aligned PEO chain helices [22–24]. However, it is more traditionally accepted that the local segmental motion of polymer chains in the flexible amorphous regions prominently controls and allows Li-ions to move inside the SPE matrix. There have been many attempts to synthesize amorphous polymer electrolytes using polymer blending [25, 26], crosslinking [27], copolymerization [28], plasticization [29–31], introducing inorganic nano–/micro–fillers [32–38], and incorporation of ionic liquids and other plasticizers [39–41]. Sometimes, just like lithium bis (trifluoromethanesulfonyl)imide (LiTFSI), if salt itself has a plasticizing effect, it could be beneficial for making flexible polymer-salt complexes [17, 18, 20, 42–47]. However, when the material becomes too plasticized as in the case of PEO–LiTFSI, the polymer electrolytes may lose free–standing properties, which should be avoided to design genuine SPEs.

The single–ion conducting polymer electrolyte has received great attention because a regular dual-ion conductor leads to a concentration gradient and cell polarization, resulting in a lower power output during discharge, higher internal impedance, and premature battery failure [48–50]. For solving these problems, the polyelectrolyte (also called an ionomer) with counter ions bound to the backbone has been a topic of interests [20, 51]. Through this approach, it is possible to achieve a cation transference number close to unity in principle. However, in general, many single-ion conductors have inferior ionic conductivity compared to dual–ion conductors because of reduced charge concentration and/or mobility [52]. For example, a PEO-poly(lithium 4-styrenesulfonate) (PLSS; also called LiPSS) complex exhibited a very low ionic conductivity ($\sigma = 3.0 \times 10^{-8}$ S/cm at 25 °C), although the Li^+-transference number ($t_{Li^+} = 0.85$ at 70 °C) was high enough [53]. To overcome this low σ, some researchers added a plasticizer into the PEO-PLSS complexes, and others designed completely new polyelectrolyte [20, 54–59].

In this study, a ternary blend composed of PEO, LiTFSI and PLSS for improving the performance of binary PEO-LiTFSI and PEO-PLSS complexes was investigated. A conventional PEO-LiTFSI electrolyte is very sticky without dimensional stability in the amorphous state [42], whereas a single-ion conductor PEO-PLSS has a small ionic conductivity ($\sigma = \sim 10^{-8}$ S cm^{-1}) [53]. To solve these problems, the ternary complexes with different [EO]:[Li^+] molar ratios were prepared in order to have a balance property among ionic conductivity, transference number and mechanical stability. Then, the optical, thermal, structural, and electrochemical properties of SPE materials were examined. The melting point depression phenomena [60, 61] were observed when the ternary composition was changed. The temperature dependence of ionic conductivity was analyzed in terms of the empirical Vogel-Tammann-Fulcher (VTF) equation [62–64]. As a result, the prefactor (A), empirical constant (B), and pseudo activation energy (E_a) were obtained. Then the electrochemical stability window and Li^+–transference number were characterized. Finally, the charge-discharge properties were examined using the Li/SPE/$LiFePO_4$ cell.

Experimental

Materials

PEO ($Mw = 5 \times 10^6$ g/mol, Aldrich) was dried overnight at 50 °C under vacuum in order to remove the butylhydroxytoluene (BHT) stabilizer. LiTFSI (Aldrich) was dried at 150 °C for 24 h before use. Poly(sodium 4-styrenesulfonate) ($Mw = 7 \times 10^4$ g/mol), lithium hydroxide monohydrate ($LiOH{\cdot}H_2O$), tetrahydrofuran (THF), ethyl alcohol, acetonitrile, $LiFePO_4$, and N-methyl-2-pyrrolidone (NMP) were purchased from Aldrich. Super-P (Imerys, Switzerland), and dimethyl sulfoxide (DMSO) (Duksan Chemicals) were used as received. Air sensitive reagents and procedures were managed in the argon-filled glove box.

Preparation of polymer electrolyte

PLSS was synthesized using ion exchange method according to literature report [53]. The solutions of PEO/LiTFSI/PLSS were prepared in the glove box. PEO was first dissolved in acetonitrile overnight. Then LiTFSI and PLSS were added into the solution and then stirred further for 24 h. Then, this viscous electrolyte solution was poured on a Teflon plate and left to evaporate acetonitrile slowly at 30 °C, leading to a self-standing film. The prepared thin-film was dried under high vacuum at 60 °C for 24 h to remove any residual solvent. The thickness of the film ranged from 85–120 μm. PEO, LiTFSI and PLSS were mixed in molar ratio of $[EO]_x$: $LiTFSI_y$: $[LSS]_z$, where x = 10, 12, 14, 16, 24, and 40; y = 1; and z = 1, leading to [EO]:[Li^+] = ratios of 5:1, 6:1, 7:1, 8:1, 12:1

and 20:1. Here, EO and LSS stand for the structural repeat units of PEO and PLSS, respectively. [Li^+] denotes Li^+ ions ionized from both LiTFSI and PLSS.

Preparation of composite cathode

The composite cathode was prepared by dissolving in NMP, the components of $LiFePO_4$, [EO]:LiTFSI: [LSS] = 14:1:1 complex (as a binder and Li-ion conductor), and Super-P with the ratio of 70:20:10 (wt.%). After ball milling for 3 h, the slurry solution was coated on 15 μm thick aluminum foil and dried under vacuum at 110 °C for 12 h. The electrode was pressed with a roll pressed machine (WV-60, Samyang 60, Korea) and then punched into a circular disc of 7 mm radius. The active mass loading of the positive electrodes was 4.2 mg cm^{-2}. Together with SPE and the Li metal as a counter/reference electrode, the composite positive electrode was assembled with a CR-2032 coin–type half–cell in the argon glove box for charge-discharge cycling performance measurements.

Materials characterization

Chemical structures (functional groups) were identified using Fourier-transform infrared spectroscopy (FT-IR, Nicolet iS5, USA). Thermal analyses were carried out using differential scanning calorimetry (DSC, Mattler-Toledo STAR^e system, version 12.1) under N_2 at the scanning rate of 10 °C min^{-1}. An x-ray diffractometer (XRD, Rigaku Smartlab, Japan) was used to figure out the crystallinity of SPE under Cu-Kα (=1.5406 Å) radiation at 40 kV and 40 mA. The morphologies of SPE were investigated using field-emission scanning electron microscope (FE-SEM, Hitachi S-4800, Japan) at 5 kV electron beam energy. All the electrochemical performances were carried out using Autolab electrochemical workstation (ECO CHEMIE, PGSTAT 100). Some properties of materials were characterized while the electrochemical cell was placed in an oven. Electrochemical impedance spectroscopy (EIS) measurements were also carried out to obtain Nyquist plots, leading to the calculation of ionic conductivity of a sample. The EIS spectra were characterized at different temperatures (~25–90 °C) with an applied potential difference of 10 mV and frequency range of 0.01 Hz to 10^6 Hz. The free-standing SPE samples were inserted between two stainless-steel electrodes with an active area of 1 × 1 cm^2 and then compacted inside a pouch cell using vacuum sealer. Linear sweep voltammetry (LSV) was carried out to determine the electrochemical potential window of the SPE samples, for which stainless steel and Li metal foil were used as working and counter (reference) electrodes, respectively. The voltage was swept from 0 to 7 V versus Li/Li^+ with a scanning rate of 1 mV s^{-1} at room temperature. The transference number of Li-ion (t_{Li^+}) was estimated using the steady-state current method. The electrolyte was inserted between two Li metal electrodes and assembled with a CR-2032 coin type cell in the glove box. The Li metal surface was scraped and cleaned with a scalpel prior to putting the components together in the coin cell. The AC impedance measurement was conducted before and after potentiostat polarization at 70 °C [53, 54]. The symmetric cell was polarized by applying a constant voltage of 10 mV. The charge-discharge dynamic performance of the $Li/SPE/LiFePO_4$ coin type half–cell was analyzed using a TOSCAT–3000 battery charge/discharge test system (Toyo System Co., Ltd, Japan). The half–cell was assembled in the glove box and then stored in a vacuum oven at 50 °C for 12 hr in order to enhance interfacial contact between the SPE and the composite positive electrode. The charge–discharge cycle property of the cell was analyzed using a constant current and constant voltage (CC–CV) input charging method with different *C*-rates (0.1 *C*, 0.2 *C*, 0.5 *C* and 1.0 *C*) and then discharges at the same rate with a voltage range of 3–4.5 V.

Results and discussion

Chemical structures and FT-IR spectra analysis

Figure 1 shows the chemical structures of PEO, LiTFSI, and PLSS, in which PEO is a polar polymer with the donicity of ~20 to provide excellent solubility for Li salts [16], LiTFSI is a plasticizing salt with well delocalized anions, and PLSS is a polyelectrolyte/ionomer with bound anions in the sulfonate group. These molecules comprise the main components of the ternary SPE in this work.

Figure 2(a) shows the FT-IR spectra for PLSS sample, in which the prominent peaks at 1500 cm^{-1} and 1430 cm^{-1} reveal the S=O antisymmetric vibration. The peaks at 1070 cm^{-1} and 833 cm^{-1} are attributed to the symmetric vibration of S–O. This result suggests that PLSS was successfully synthesized [53, 65]. Figure 2(b) shows the FT-IR spectra of various polymer electrolytes at different salt, PLSS and LiTFSI composition. From pure PEO, the characteristic vibrational peaks exhibits an asymmetric aliphatic C-H stretching mode at 2877 cm^{-1}, CH_2 asymmetric scissoring mode at ~1466 and 1454 cm^{-1}, CH_2 wagging mode at 1340 and 1360 cm^{-1}, CH_2 asymmetric twisting at 1279 and 1240 cm^{-1}, CH_2 asymmetric rocking at 960 and 946 cm^{-1}(shoulder type) , C–O stretching and CH_2 rocking mode at 841 cm^{-1}, and strong C–O–C stretching bands which are splits into three peaks at ~1143 cm^{-1}, 1093 cm^{-1}, and 1059 cm^{-1}, respectively [66]. The

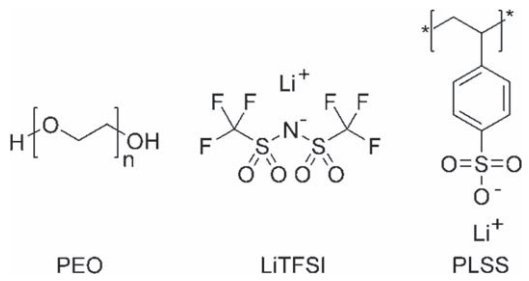

Figure 1. Chemical structures of PEO, LiTFSI, and PLSS.

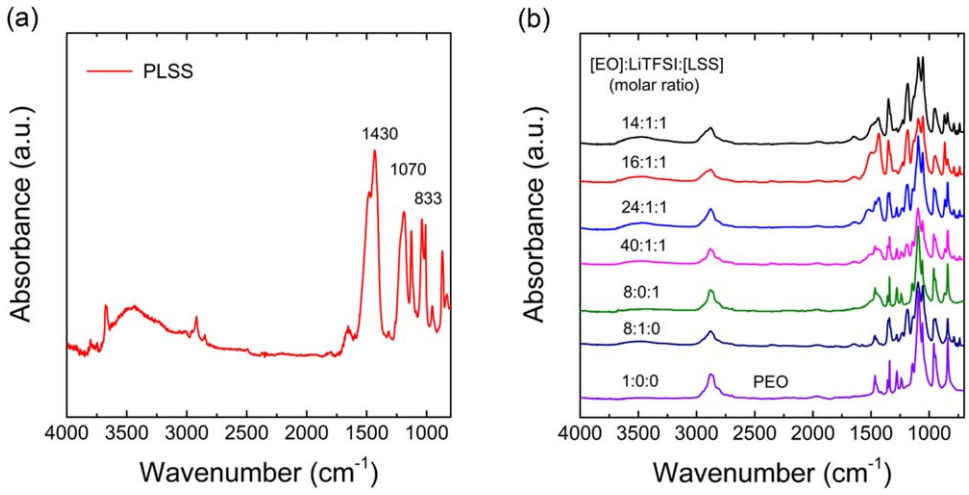

Figure 2. FT-IR spectra of (a) PLSS and (b) PEO-LiTFSI-PLSS composite. Here, [EO] and [LSS] indicate the structural (repeat) units of PEO and PLSS, respectively.

presence of CH_2 bending vibrations and C–O–C triplet peaks demonstrates the presence of PEO crystallinity [67].

With the addition of LiTFSI and PLSS into PEO, the change in intensity and position of spectral patterns are notably observed. The CH_2 asymmetric scissoring peak has excessively broadened, implying interaction between PEO chains and the added salts. It was observed that the spectra is first largely influenced by the concentration of PLSS, which corresponds to PEO-PLSS blend and it was found to be broader as the concentration of PLSS and LiTFSI increases [68]. The triplet stretching peaks from C–O–C ether linkages became wider and shifted down to 1132 cm^{-1}, 1093 cm^{-1}, and 1055 cm^{-1} with increasing salt concentration which is attributed to the complexation of cations with ether oxygen. As a result, the intensity of CH_2 asymmetric twisting spectra also decreased and downshifted to lower wavenumbers and the CH_2 asymmetric rocking modes became a single less intense band that appears at about 949 cm^{-1}. These observations indicate that the mixing remarkably enhanced the overall disordered conformation of PEO chain molecules [69, 70].

The new peak observed at 1184 cm^{-1} is ascribed to the TFSI anion's plasticizing effect within the polymer electrolyte complex [71]. The sharp peak at 841 cm^{-1} which corresponds to C–O stretching and CH_2 rocking modes became broaden and split into two peaks, appearing at 866 and 843 cm^{-1}. In the spectrum of the PEO-LiTFSI complex, a set of three peaks were observed at 785 cm^{-1}, 761 cm^{-1}, and 734 cm^{-1} due to the S–N–S asymmetric vibration, the CF_3 asymmetric bending vibration mode, and the S-N-S symmetric stretching mode, respectively. This absorption slightly shifted to higher wavenumbers in the PEO-LiTFSI-PLSS blend and appeared at 786 cm^{-1}, 761 cm^{-1}, and 738 cm^{-1}. The little broadening of the symmetric S-N vibration indicates LiTFSI is well dissolved into the host polymer, PEO.

Thermal property and melting point depression

Solid to liquid (S–L) phase transition is the melting of crystalline regions, increasing additional active segmental motions in amorphous regions. Figure 3 shows the DSC thermograms for the SPE samples in the range of –50 to 100 °C, in which –50 °C was limited by the DSC instrument itself although PEO's T_g is known to be about –60 °C [13, 15–19]. The melting points were taken at the peak maximum. Figure 3(a) shows the different roles between

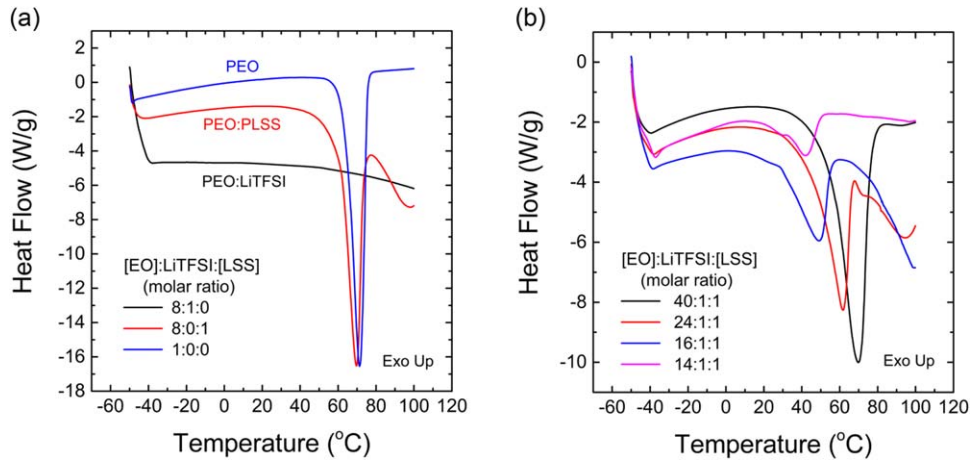

Figure 3. DSC thermograms: (a) PEO, PEO-PLSS, and PEO-LITFSI. (b) PEO-LiTFSI-PLSS composites.

LiTFSI and PLSS when blended with PEO. Interestingly, there is no S–L transition of PEO in PEO-LiTFSI with [EO]:[Li^+] = 8:1, whereas the S-L transition exists in PEO-PLSS with the same molar ratio, indicating that LiTFSI destroyed the crystalline regions of PEO completely, but PLSS could not. The reasons could be found thermodynamically. PLSS has a high molecular weight just like PEO. Hence, there is no gain in the entropy of mixing ($\Delta S_m \approx 0$), but only a penalty of the mixing enthalpy ($\Delta H_m > 0$). The increased Gibbs energy of mixing, $\Delta G_m \approx \Delta H_m > 0$ (when $\Delta S_m \approx 0$), causes the binary PEO-PLSS to become phase–separated when mixed, which allows semicrystalline PEO to survive with some amounts of crystalline regions. Here, it is noteworthy that not only single-phase but also phase-separated polymer blends could be used in many practical applications [72–74]. It is clearly observed that the melting temperature of PEO in a ternary system was depressed when mixed with both LiTFSI and PLSS. The reason is that the presence of Li salts, acting as diluent or impurity from the viewpoint of PEO, may shift the S-L phase equilibrium point between the liquid and the crystalline chains of PEO, although LiTFSI and PLSS have different intermolecular interactions with PEO chains. Finally, the results of the melting point depression in the ternary PEO-LiTFIS-PLSS system were clearly plotted in figure 4 based on the data in figure 3(b). As shown in figure 4, the melting point depression is relatively small up to 20 wt.% [Li^+] salts. However, with increasing [Li^+] wt.%, the melting points are drastically depressed.

The crystallinity (χ_c) of PEO-LiTFSI-PLSS samples can be quantified from the DSC melting enthalpy (ΔH_m) data using the following equation:

$$\chi_c = \frac{\Delta H_m}{\Delta H_m^0 wf} \times 100\ \% \tag{1}$$

where ΔH_m^0 is the enthalpy of melting from the phase transition of the pure PEO crystalline region, 203 J g^{-1} (100% crystalline) [75], and *wf* is the weight fraction of PEO in a blend sample. The values of ΔH_m and χ_c of all electrolytes are presented in table 1. The addition of PLSS reduced slightly the crystalline phase, inducing the melting point depression of PEO from 71 to 69 °C. However, in the case of LiTFSI, it can destroy the crystallinity region of PEO effectively, leading to greater enhancement of the amorphous phase of PEO, although the segmental motion of disordered PEO chains could be affected by Li^+-PEO complexations, i.e. a kind of transient crosslinking. Here, the melting temperature of the ternary mixture shifted down to lower temperature with increasing [Li^+] salts, LiTFSI and PLSS. Concomitantly, the area of the peak also was reduced, leading to enthalpy of melting from 18.44 J g^{-1} (16:1:1) to 8.86 J g^{-1} (14:1:1) for the [EO]:LiTFSI:[LSS] molar ratios, indicating that, through varying the composition, we may control the amorphous phase amounts for enhancing the ionic conductivities of SPEs.

Crystal structure analysis through XRD patterns

The XRD data for the blend polymer electrolytes is illustrated in figure 5. The x-ray pattern of pure PEO reveals two strong crystalline peaks at 19.1° and 23.2°, corresponding to (120) and (032) crystallographic planes, respectively [76]. This observation indicates that the PEO host is semicrystalline. The peak intensity was reduced and widen upon the addition of LiTFSI and PLSS salts. For low concentrations of LiTFSI and PLSS salt, the intensity of the second characteristic peak of PEO at $2\theta = 23.2°$ was mainly affected and turned into broaden and short peak.

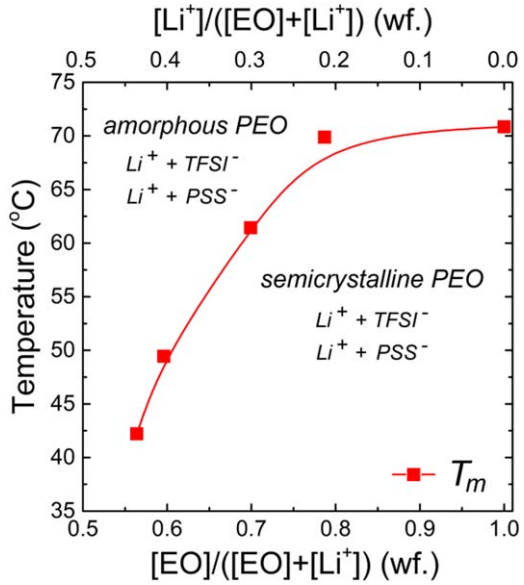

Figure 4. Phase behavior of PEO-LiTFSI-PLSS complexes, in which melting point depression is observed as a function of [EO] or [Li^+] weight fraction. Here, [Li^+] = LiTFSI + [LSS]. PSS^- denotes the poly(4-styrene sulfonate) anions, and $TFSI^-$ is the anions from LiTFSI.

Table 1. Thermal properties of the polymer blends used as SPE.

[EO]:LiTFSI:[LSS] (molar ratio)	T_m (°C)	ΔH_m (J/g)	$wf(-)$	χ_c(%)
1:0:0	71.13	156.8	1.00	77.24
8:0:1	69.47	66.20	0.65	50.21
40:1:1	69.85	78.91	0.79	49.41
24:1:1	61.58	31.28	0.69	22.37
16:1:1	49.16	18.44	0.60	15.24
14:1:1	42.25	8.86	0.56	7.75

As can be seen from the figure 5, the two PEO peaks became relatively broader as well as less prominent as the LiTFSI and PLSS content increased in PEO. This reveals that Li^+ ion and C–O–C segment coordination interaction alters the ordered arrangements PEO chains while promoting salt dissociation and increasing charge carriers. The absence of sharp peaks in the [EO]:LiTFSI:[LSS] = 14:1:1 indicates that PEO exhibits no crystalline characteristics and suggests a complete dissolution of the salts into PEO host matrix. This observation is consistent with the information obtained from DSC. Note that the crystallite size (t) could be calculated based on Scherrer's equation [77, 78],

$$t = \frac{0.9\lambda}{\beta \cos\theta} \tag{2}$$

where λ (=0.154 nm) is the x-ray wavelength, β is the full width at half maximum (FWHM), and θ is the diffraction angle of x-ray light. As shown in table 2, although other component can destroy the PEO's crystalline regions (i.e. decrease of crystallinity), the crystallite size (average single crystalline domains in polycrystals) slightly increases when blended.

Ionic conductivity and Vogel-Tammann-Fulcher equation

Electrochemical Impedance Spectroscopy was performed to study the ionic conductivity of polymer electrolytes at different salt concentration using the device with a stainless steel (SS)/SPE/SS configuration [see the inset of figure 6(a)]. Figure 6(a) shows the ionic conductivity as a function of salt concentration. As displayed in figure 6(a), at a low concentration of salts such as [EO]/[Li^+] = 20 (or [EO]:LiTFSI:[LSS] = 20:0.5:0.5 = 40:1:1), the electrolyte has a high resistivity owing to the small concentration of charge carriers and the limited segmental motion of PEO chains coming from a significant crystallinity, χ_c = ~22.37%–49.41% (see table 1). On the other hand, at a high concentration of salts such as [EO]/[Li^+] > 5, the SPE shows also a high resistivity, probably owing to ion association and decrease of entropy originating from a high fraction of rigid salts in a ternary blend. Hence,

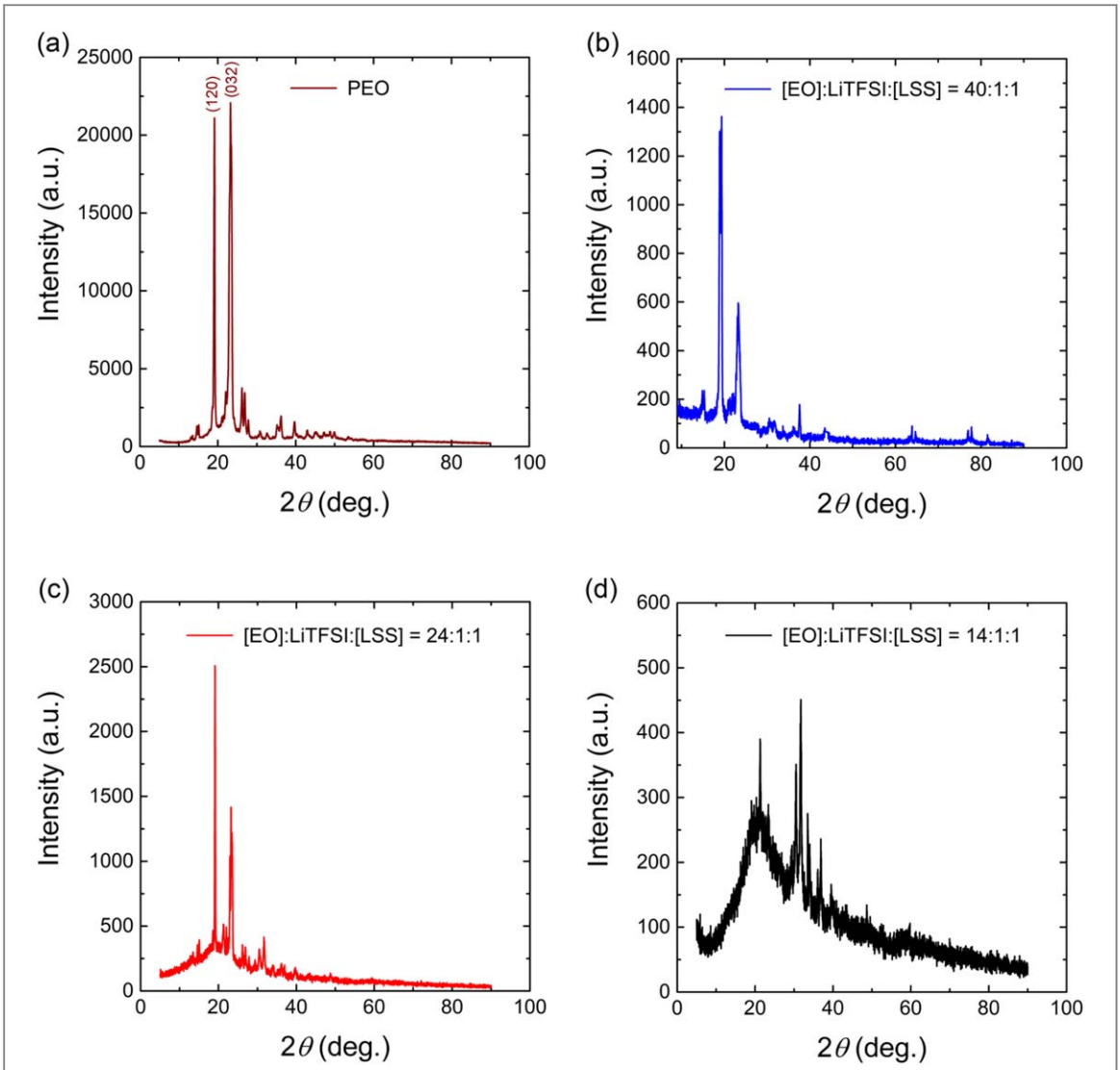

Figure 5. XRD diffraction patterns of (a) PEO, (b) [EO]:LiTFSI:[LSS] = 40:1:1, (c) [EO]:LiTFSI:[LSS] = 24:1:1, and (d) [EO]:LiTFSI:[LSS] = 14:1:1.

Table 2. Crystallite size (t) of (120) crystallographic planes of PEO in PEO-LiTFSI-PLSS blends as a function of composition. Here, d-spacing is calculated based on Bragg's law: $\lambda = 2d \sin\theta$.

[EO]:LiTFSI:[LSS] molar ratio	2θ(°)	θ(°)	β(radians)	t(nm)	d-spacing (nm)
1:0:0	21.28	10.64	0.00375	39.50	0.25
40:1:1	19.38	9.69	0.00315	44.64	0.42
24:1:1	19.10	9.55	0.00239	58.81	0.42
14:1:1	19.14	9.57	0.00459	30.62	0.42

in this work, at an intermediate concentration of salts such as [EO]/[Li^+] = ~6–8 (or [EO]:LiTFSI:[LSS] = ~6–8:0.5:0.5 = ~12–16:1:1), the SPE showed higher ionic conductivity. Specifically, at [EO]/[Li^+] = 7, σ was highest, 1.7×10^{-5} S cm^{-1}, indicating that there is an effective segmental motion of PEO-Li^+ complexes with relatively small $\chi_c \approx 7.75\%$.

Figure 6(b) shows the logarithmic ionic conductivity of the polymer electrolyte at different compositions as a function of reciprocal temperature. As the temperature increased from 298.15 K to 363.15 K, the ionic conductivity of all electrolytes increased nonlinearly because of (1) the increased movement of PEO segments and their complexed ions in the ternary PEO-LiTFSI-PLSS system, (2) the increased amorphous regions at $T > 328.15$ K = 55 °C (here, PEO melting starts; see figure 3(a)), and (3) a potential dissociation of aggregated ions. Specifically, when the PEO component is relatively large, e.g. [EO]:LiTFSI:[LSS] = 40:1:1 (pink inverse triangles) or 24:1:1 (blue triangles), we observed a noticeable transition in the ionic conductivities with respect to

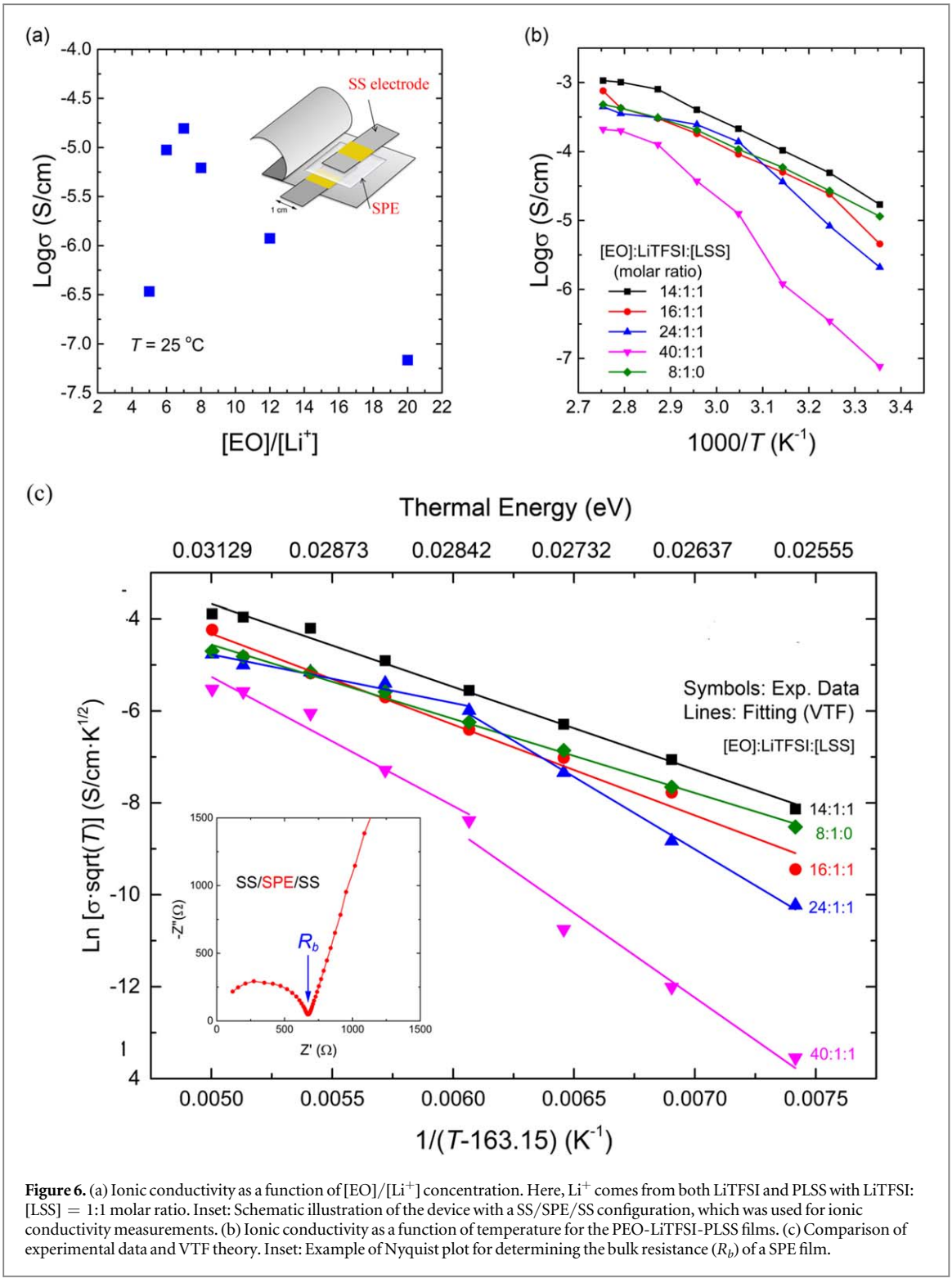

Figure 6. (a) Ionic conductivity as a function of [EO]/[Li^+] concentration. Here, Li^+ comes from both LiTFSI and PLSS with LiTFSI: [LSS] = 1:1 molar ratio. Inset: Schematic illustration of the device with a SS/SPE/SS configuration, which was used for ionic conductivity measurements. (b) Ionic conductivity as a function of temperature for the PEO-LiTFSI-PLSS films. (c) Comparison of experimental data and VTF theory. Inset: Example of Nyquist plot for determining the bulk resistance (R_b) of a SPE film.

temperature as shown in figure 6(b). This is because, when the crystallinity of ternary SPE is relatively high (χ_c= 49.39% and 22.37% for [EO]:LiTFSI:[LSS] = 40:1:1 and 24:1:1, respectively), there is a significant expansion of free volumes during the melting transition at ~328.15–348.15 K (=~55 °C–75 °C). On the other hand, when $\chi_c < 20\%$, the transition of ionic conductivity is not readily discernable at the aforementioned melting range, owing to a relatively minor increase of amorphous regions.

When the temperature is higher than 1.15 × T_g (e.g. PEO: 1.15 × 213.15 = 245.15 K), it is known that VTF equation could be applied to the explanation of log σ versus $1000/T$ plot. As shown in figure 6(b), the plots have non-constant slopes along each line of the measured conductivities, suggesting that the ionic conductivity is supported by the inter- and intra-chain segmental motion of the polymer, i.e. obeys the VTF conduction mechanism. Due to this observation, to understand the ionic transport process in the PEO-LiTFSI-PLSS

Table 3. Physical constants of VTF theory for the PEO-LiTFSI-PLSS system as a function of composition. Equilibrium glass transition temperature of PEO, $T_0 = T_g - 50 = 213.15-50 = 163.15$ K; Boltzmann constant, $k = 8.61739 \times 10^{-5}$ eV K^{-1}; Gas constant, $R = 8.31451$ J/(mol·K); and pseudo activation energy, $E_a = B \cdot k$. Note that [EO]:LiTFSI:[LSS] = 14:1:1 corresponds to [EO]:[Li$^+$] = 7:1.

	[EO]:LiTFSI:[LSS] (molar ratio)						
VTF parameters at $T_0 = 165.15$ K	14:1:1	16:1:1	24:1:1 ($T \geqslant 328.15$ K)	24:1:1 ($T \leqslant 328.15$ K)	40:1:1 ($T \geqslant 328.15$ K)	40:1:1 ($T \leqslant 328.15$ K)	8:1:0
A (S/cm·K$^{1/2}$)	206.0338	260.9790	1.6562	462485.2761	6562.0609	778987.2830	33.4162
B (K)	1800.5879	1976.6896	1055.2025	3150.5898	2809.1152	3686.4339	1613.4263
E_a (eV)	0.1552	0.1617	0.0909	0.2715	0.2421	0.3358	0.1390
E_a (kJ/mol)	14.9710	15.6038	8.7735	26.1956	23.3564	32.3969	13.4149

electrolyte, we employed VTF equation [62, 63],

$$\sigma = AT^{-1/2} \exp\left(-\frac{B}{T - T_0}\right) \tag{3}$$

where A, B, and T_0 are a prefactor, an empirical constant with unit of temperature (related with expansivity), and the equilibrium glass transition temperature (called Vogel temperature), respectively. Here, T_0 is known to be smaller than the glass transition temperature (T_g) by ~45–50 K [43, 62, 63]. In this work, we used $T_0 = T_g - 50$ K [43, 62]. At this moment, it is noteworthy that, until now, most authors have obtained the three VTF parameters (A, B, and T_0) through simple fitting methods [16, 62, 79]. However, in this work, we used PEO's T_g (=213.15 K) [15–19] for estimating T_0 (=213.15−50 = 163.15 K), and obtained the other two VTF parameters (A and B) through a fitting method. From B, we may estimate pseudo activation energy ($E_a = B \times k$) analogous to the activation energy, in which $k = 8.61739 \times 10^{-5}$ eV K^{-1} is Boltzmann constant. Thus, based on the data in figure 6(b), we fitted the data using the plot of $\ln(\sigma \cdot \sqrt{T})$ versus $1/(T - 163.15)$ and extracted the VTF parameters, A and B (see figure 6(c)). The results are summarized in table 3. Note that for [EO]:LiTFSI:[LSS] molar ratios of 40:1:1 or 24:1:1, we fitted the data with two separate ranges, i.e. $T \geqslant 328.15$ K and $\leqslant 328.15$ K, because of a noticeable transition in σ due to the melting of PEO around this temperature. However, for the case of the other compositions, we fitted in the data using the full range of temperatures from 298.15 to 363.15 K. As shown in table 3, when $\sigma = 1.7 \times 10^{-5}$ S cm^{-1} at the composition of [EO]:LiTFSI:[LSS] = 14:1:1, i.e. [EO]:[Li$^+$] = 7:1, the VTF parameters are $A = 206.0338$ S cm^{-1}·K$^{1/2}$, $B = 1800.5879$ K, and $E_a = 0.1552$ eV or 14.8710 kJ mol^{-1}. However, when $\sigma = 7.6 \times 10^{-8}$ S/cm at the composition of [EO]:LiTFSI:[LSS] = 40:1:1, i.e. [EO]:[Li$^+$] = 20:1, the VTF parameters ($T \leqslant 328.15$ K) are $A = 778987.2830$ S cm^{-1}·K$^{1/2}$, $B = 3896.4339$ K, and $E_a = 0.3358$ eV or 32.3969 kJ/mol. Note that the pseudo activation energy are increased more than a factor of two when the composition was changed from [EO]:[Li$^+$] = 7:1 to 20:1, indicating that the expansivity of free volumes in PEO-LiTFSI-PLSS is very restricted when [EO]:[Li$^+$] = 20:1. Finally, it is notable that, although we used A as a fitting parameter in the plot of $\ln(\sigma \cdot \sqrt{T})$ versus $1/(T - 163.15)$, its physical meaning could be found from the relationships, $\sigma = nq\mu = nq(q/kT \cdot D)$, $D = CT^{1/2}[-B/(T - T_0)]$, and in which n is the concentration of charge, q is charge, μ is mobility, D is diffusion coefficient, and C is a constant. Hence, A is physically related with the concentration of charges. However, the constant C is unknown, making it difficult to compare across systems as a function of composition.

Li-ion transference number

The lithium-ion transference number (t_{Li^+}) was calculated according to the equation initially proposed by Evans *et al* [80]

$$t_{Li^+} = \frac{I^S(\Delta V - I^0 R_I^0)}{I^0(\Delta V - I^S R_I^S)} \tag{4}$$

ΔV is the DC potential applied across the cell, I^0 and I^S are the initial and steady-state currents, R_I^0 and R_I^S are the initial and steady-state interfacial resistance measured by the AC impedance method before and after DC polarization, respectively. The ion transference number, which describes the fraction of current carried by a particular ionic species, is just as important as the total conductivity. Increasing the cation transference number close to one may provide a long-lasting battery lifetime. A conventional PEO-LiTFSI complex has shown a poor lithium ion transference number between 0.16–0.30, being independent of temperature [43], whereas PEO-PLSS has a high transference number, 0.85 at 70 °C [53].

Figure 7(a) shows the current variation as a function of time during DC polarization of the Li/SPE/Li symmetrical cell subjected to a voltage, ΔV (=0.01 V), at 70 °C [53, 54, 81] and the two AC impedance spectra to measure the interfacial resistance before polarization I^0(=1.626 × 10^{-5}A) and after a steady state current has

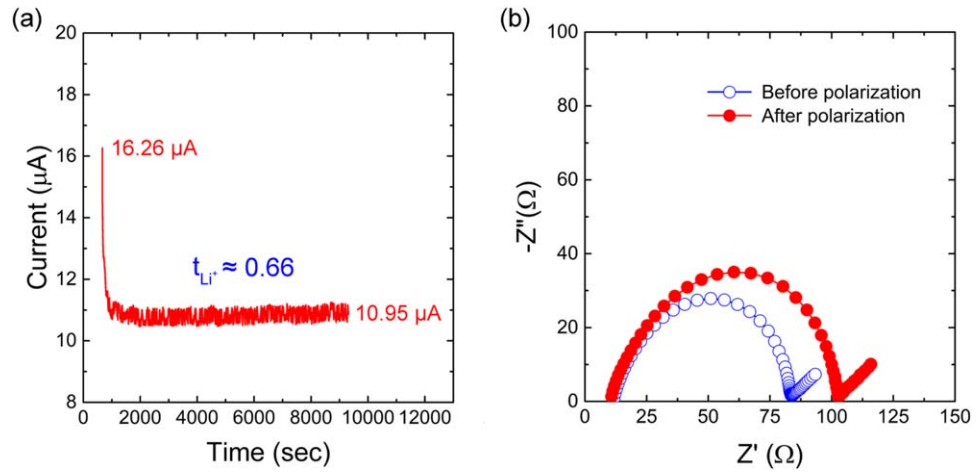

Figure 7. (a) The current response of Li/SPE/Li cell as a function of time during DC polarization under a constant potential of 0.01 V. (b) The AC impedance spectra of the same cell measured at 70 °C before and after DC polarization.

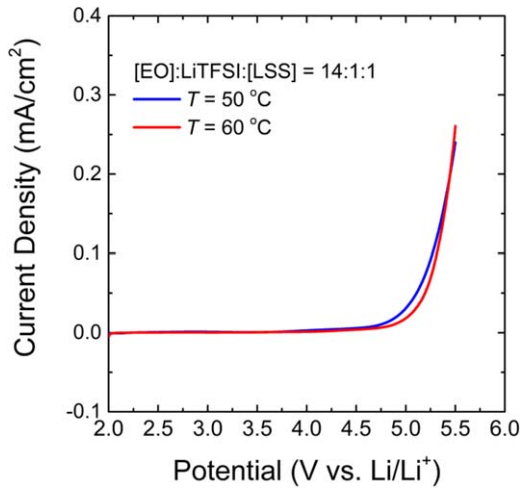

Figure 8. Linear sweep voltammogram of PEO-LiTFSI-PLSS polymer electrolyte.

been reached I^S(=1.095 × 10^{-5}A). Then $t_{Li^+} \approx 0.66$ was calculated using equation (4) based on R_1^0(=71.934 Ω) and R_1^S(=91.724 Ω) in figure 7(b). Briefly, when the DC voltage was applied to the Li/SPE/Li cell, Li^+ cations migrated toward the cathode but $TFSI^-$ anions migrated to the anode and accumulated at the electrolyte-electrode interface. Here, note that in the case of styrene sulfonate anions, it could not migrate over a long range because anions were bound to the polyelectrolyte. Then, after steady state reached, only Li^+ cations could migrate. Hence, by measuring the electrical properties before and after this DC polarization, we may estimate t_{Li^+}. Accordingly, the [EO]:LiTFSI:[LSS] = 14:1:1, i.e. [EO]:[Li^+] = 7:1 blend, has $t_{Li^+} \approx 0.66$, indicating that the cation mobility is higher than that of counter anions. This is because PSS anions are fixed on the polymeric chains and partially disrupt the ordering of the PEO matrix, although PEO and PLSS are in a phase-separated state. Recall that, because of entropic reasons, the polymer-salt PEO-LiTFSI complex is much more miscible than the polymer-polyelectrolyte PEO-PLSS complex.

Electrochemical stability window analysis through linear sweep voltammetry

The electrochemical stability of the polymer electrolyte was measured by linear sweep voltammetric (LSV) measurements at 50 °C and 60 °C, respectively. Figure 8 presents the LSV curve of the blended electrolyte (sandwiched) on a Li/SPE/SS coin type cell assembled inside a glove box. It is observed that the anodic stability of the blend solid polymer electrolyte (namely, the onset voltage for oxidative decomposition) is at ~4.7 ± 0.1 V (Li versus Li^+), indicating that the electrochemical stability window of this polymer electrolyte is suitable for practical applications.

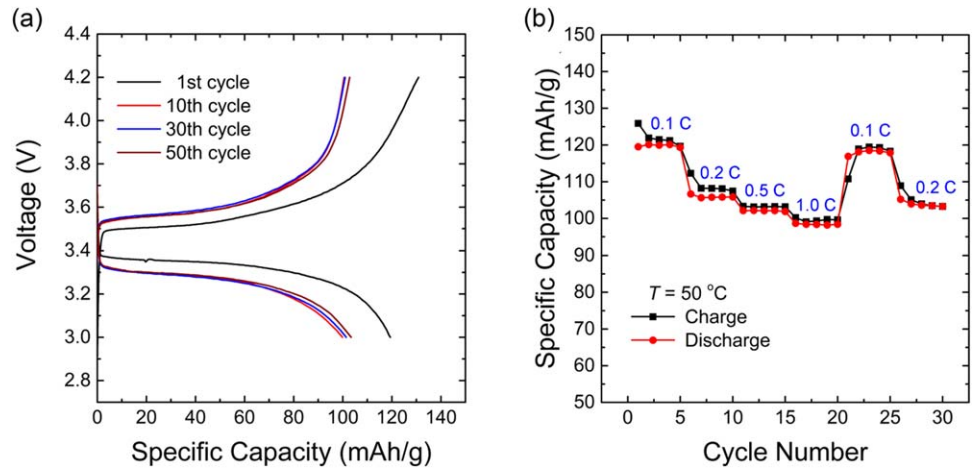

Figure 9. (a) Charge-discharge profile of Li/SPE/$LiFePO_4$ cell at 50 °C. (b) Specific capacities of cell during charge and discharge at different *C*-rates at 50 °C.

Charge-discharge cycling performance

To assess the performance of PEO-LiTFSI-PSS electrolyte in a practical battery, we assembled a coin type half-cell inside a glove box with the Li/SPE/$LiFePO_4$ configuration. Hence, the cell has a Li metal electrode, composite positive electrode ($LiFePO_4$), and free-standing SPE as electrolyte and separator. Figure 9(a) shows the charge discharge curve of the cell for different cycle numbers at 50 °C. The smooth horizontal potential plateau starts at about 3.4 V, related with the intercalation/deintercalation of Li^+ into the $LiFePO_4$ structure, leading to stable and reversible cycles. The charge-discharge specific capacities at different *C*-rate are shown in figure 9(b). Here, *C*-rate is defined by $C = I/f$, in which I is current and f is a multiple or a fraction of *C*. For example, if discharged at a current of 12.1 mA in the 121 mAh/g cell, the *C*-rate would be 0.1*C*, indicating *C*-rate is equivalent to current [82]. The specific capacities were found to be 121 mAh g^{-1}, 105 mAh g^{-1}, 102 mAh g^{-1}, and 100 mAh g^{-1} at 0.1*C*, 0.2*C*, 0.5*C* and 1*C*, respectively. The corresponding coulombic efficiency began at 87%, which was lower compared to the subsequent cycle efficiencies due to irreversible processes associated with electrolyte decomposition during solid-electrolyte-interface formation. The efficiency improved and increased quickly above 98%, attributed to the high Li^+ ion transference number and ionic conductivity of the PEO-LiTFSI-PLSS polymer electrolyte. It reached close to 100% when the discharge current density returned to 0.1 *C*, indicating excellent capacity recovery and reversible lithium deposition-stripping performance.

Single-ion conducting solid polymer electrolyte: optimization

Figures 10(a) and (b) display the macroscopic and microscopic SEM images of the ternary PEO-LiTFSI-PLSS film, in which the former demonstrates a semi-translucent free-standing property and the latter exhibits a microscale wrinkled morphology coming from phase-separated semicrystalline PEO and a polyelectrolyte PLSS [recall DSC data in figure 3(b)]. Finally, figure 10(c) sums up this research through the schematic illustration about the concept of this work. In this triangle, the maximum area indicates the ideal single-ion conducting SPE with characteristics of high ionic conductivity, high transference number, and free-standing properties. However, note that in this triangle, we do not compare other important factors such as the stability window and electrolyte-electrode interfacial kinetics. As shown in this scheme, the binary polymer electrolyte systems, PEO-PLSS and PEO-LiTFSI, have serious drawbacks in ionic conductivity and mechanical properties, respectively. Therefore, by combining these together through a ternary approach, we could optimize the property of this SPE, demonstrating that the ternary SPE approach is promising in the development of SPEs.

Conclusions

We demonstrated that a ternary PEO-LiTFSI-PLSS complex is an optimized system in terms of overall ionic conductivity, transference number and free-standing mechanical properties, when compared to a binary PEO-LiTFSI (a sticky film without free-standing property in amorphous state) or PEO-PLSS (with small $\sigma \sim 10^{-8}$ S cm^{-1}). In this study, the major findings are as follows: (1) In the DSC data, we observed melting point depression and the crystallinity of the [EO]:[Li^+] = 7:1 complex is 7.75%. (2) Through XRD patterns, we observed that the small molecule LiTFSI salt/ions effectively destroyed the crystalline regions of PEO when compared to a polyelectrolyte PLSS. Note that polymer-polyelectrolyte is not as miscible as observed in other

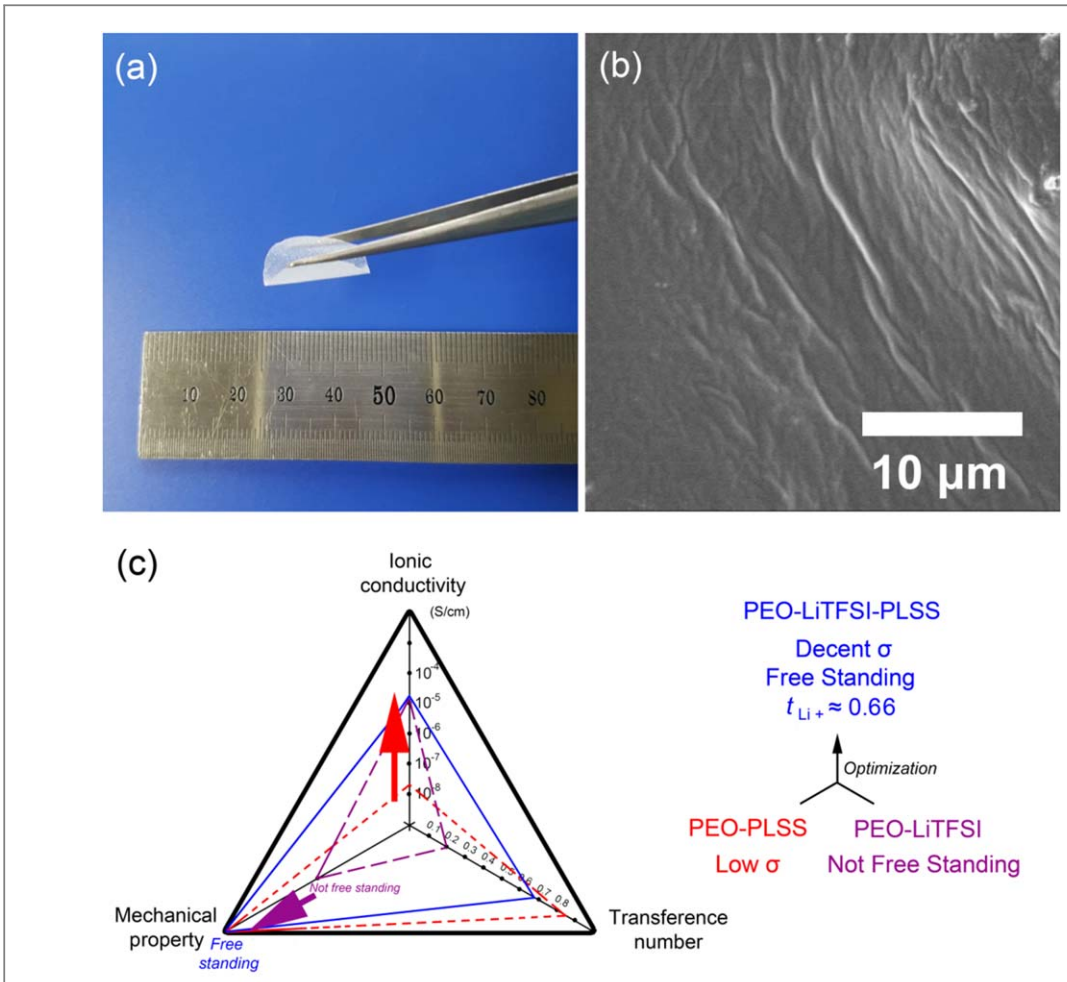

Figure 10. (a) Macroscopic and (b) microscopic SEM images of the ternary PEO-LiTFSI-PLSS film. (c) Schematic illustration for optimizing the SPEs by comparing three polymer electrolyte complexes: ternary PEO-LiTFSI-PLSS (blue line), binary PEO-PLSS (red), and binary PEO-LiTFSI (purple).

polymer-polymer blends if there is no specific interaction. (3) The ionic conductivities of the [EO]:[Li^+] = 7:1 complex were 1.70 × 10^{-5} S cm^{-1} at 25 °C and 1.04 × 10^{-4} S cm^{-1} at 45 °C. (4) For explaining the temperature dependency of ionic conductivity, the VTF equation was employed, resulting in the VTF parameters of A = 206.0338 S cm^{-1} $K^{1/2}$, B = 1800.5879 K, and E_a = 0.1552 eV for the [EO]:[Li^+] = 7:1 complex. (5) The ternary PEO-LiTFSI-PLSS showed the lithium transference number, ~0.66 at 70 °C when tested with Li/SPE/Li cell using DC polarization and AC impedance methods. (6) The ternary system showed a wide enough electrochemical stability window, ca. 4.7 ± 0.1 V in the Li/SPE/SS device when analyzed by the linear sweep voltammetry method. Finally, (7) a coin type half-cell with the Li/SPE/$LiFePO_4$ configuration displayed the specific capacity of 121 mAh/g at a 0.1 C-rate, demonstrating that this free-standing electrolyte is appropriate for a practical Li-ion battery. Therefore, the ternary blends incorporating a polyelectrolyte, just like versatile polymer-polymer blend systems in commercial markets, appears promising as a material of choice, applicable for energy storage devices such as batteries and supercapacitors.

Acknowledgments

This work was supported by both Hanbat University in Korea and Jimma Institute of Technology in Ethiopia. We thank Dr Timothy Kwa for contributing in the scientific discussion on the manuscript.

Data availability statement

All data that support the findings of this study are included within the article (and any supplementary files).

Notes

The author declares no competing financial interest.

ORCID iDs

Jung Yong Kim https://orcid.org/0000-0002-7736-6858

References

[1] Goodenough J B and Park K S 2012 *J. Am. Chem. Soc.* **135** 1167–76
[2] Blomgren G E 2017 *J. Electrochem. Soc.* **164** A5019–25
[3] Manthiram A 2017 *ACS Cent. Sci.* **3** 1063–9
[4] Bruce P G, Scrosati B and Tarascon 2008 *Angew. Chem. Int. Ed.* **47** 2930–46
[5] Armand M and Tarascon J M 2008 *Nature* **451** 652–7
[6] Boaretto N, Meabe L, Martinez-Ibanez M, Armand M and Zhang H 2020 *J. Electrochem. Soc.* **167** 070524
[7] Manthiram A, Yu X and Wang S 2017 *Nat. Rev. Mater* **2** 1–16
[8] Tarascon J M and Armand M 2001 *Nature* **414** 359–67
[9] Balakrishnan P G, Ramesh R and Kumar T P 2006 *J. Power Sources* **155** 401–14
[10] Wen J, Yu Y and Chen C 2012 *Mater. Express* **2** 197–212
[11] Chen R, Qu W, Guo X, Li L and Wu F 2016 *Mater. Horiz.* **3** 487–516
[12] Fenton D E, Parker J M and Wright P V 1973 *Polymer* **14** 589
[13] Armand M 1983 *Solid State Ion.* **9 and 10** 745–54
[14] Kim J Y and Chung I J 2002 *J. Electrochem. Soc.* **149** A1376–80
[15] Takahashi Y and Tadokoro H 1973 *Macromolecules* **6** 672–5
[16] Pearce R and Vancso G J 1997 *Macromolecules* **30** 5843–8
[17] Lascaud S, Perrier M, Vallee A, Besner S, Prud'homme J and Armand M 1994 *Macromolecules* **27** 7469–77
[18] Marzantowicz M, Dygas J R, Krok F, Lasinska A, Florjanczyk Z, Zygadlo-Monikowska E and Affeck A 2005 *Electrochim. Acta* **50** 3969–77
[19] Xue Z, He D and Xie X 2015 *J. Mater. Chem. A* **3** 19218–53
[20] Lin K-J, Li K and Maranas J K 2013 *RSC Adv.* **3** 1564–71
[21] Panzer M J and Frisbie C D 2007 *J. Am. Chem. Soc.* **129** 6599–607
[22] Macglashan G S, Andreev Y G and Bruce P G 1999 *Nature* **398** 792–4
[23] Gadjourova Z, Andreev Y G, Tunstall D P and Bruce P G 2001 *Nature* **412** 520–3
[24] Stoeva Z, Martin-Litas I, Staunton E, Andreev Y G and Bruce P G 2003 *J. Am. Chem. Soc.* **125** 4619–26
[25] Stephan A M, Thirunakaran R, Renganathan N G, Sundaram V, Pitchumani S, Muniyandi N, Gangadharan R and Ramamoorthy P J 1999 *Power Sources* **81 and 82** 752–8
[26] Tao C, Gao M-H, Yin B-H, Li B, Huang Y-P, Xu G and Bao J–J 2017 *Electrochim. Acta* **257** 31–9
[27] Lee K-H, Kim K-H and Lim H S 2001 *J. Electrochem. Soc.* **148** A1148
[28] Zheng T, Zhou Q, Li Q, Zhang L, Li H and Lin Y 2014 *Solid State Ion.* **259** 9–13
[29] Das S and Ghosh A 2015 *Electrochim. Acta* **171** 59–65
[30] Al-Salih H, Huang A, Yim C-H, Freytag A I, Goward G R, Baranova E and Abu-Lebdeh Y 2020 *J. Electrochem. Soc.* **167** 070557
[31] Dhatarwal P and Sengwa R J 2020 *Compos. Commun.* **17** 182–91
[32] Croce F, Appetecchi G B, Persi L and Scrosati B 1998 *Nature* **394** 456–8
[33] Sun H, Sohn H, Yamamoto O, Takeda Y and Imanishi N 1999 *J. Electrochem. Soc.* **146** 1672–6
[34] Thokchom J S, Chen C, Abraham K M and Kumar B 2005 *Solid State Ion.* **176** 1887–93
[35] Nugent B J L, Moganty S S and Archer L A 2010 *Adv. Mater.* **22** 3677–80
[36] Liu W, Liu N, Sun J, Hsu P-C, Li Y, Lee H-W and Cui Y 2015 *Nano Lett.* **15** 2740–5
[37] Abraham K M, Koch V R and Blakley T J 2000 *J. Electrochem. Soc.* **147** 1251
[38] Tan X, Wu Y, Tang W, Song S, Yao J, Wen Z, Lu L, Savilov S V, Hu N and Molenda J 2020 *Nanomaterials* **10** 157
[39] Shin J-H, Henderson W A, Tizzani C, Passirini S, Jeong S-S and Kim K-W 2006 *J. Electrochem. Soc.* **153** A1649
[40] Appetecchi G B, Kim G T, Montanino M, Alessandrini F and Passerini S 2011 *J. Power Sources* **196** 6703–9
[41] Costa L T, Sun B, Jeschull F and Brandell D 2015 *J. Chem. Phys.* **143** 024904–9
[42] Vallée A, Besner S and Prud'Homme J 1992 *Electrochim. Acta* **37** 1579–83
[43] Gorecki W, Jeannin M, Belorizky E, Roux C and Armand M 1995 *J. Phys. Condens. Matter* **7** 6823–32
[44] Cha E H, Macfarlane D R, Forsyth M and Lee C W 2004 *Electrochim. Acta* **50** 335–8
[45] Shin J, Henderson W A, Scaccia S, Prosini P P and Passerini S 2006 *J. Power Sources* **156** 560–6
[46] Zhao Y, Tao R and Fujinami T 2006 *Electrochim. Acta* **51** 6451–5
[47] Kim G T, Appetecchi G B, Alessandrini F and Passerini S 2007 *J. Power Sources* **171** 861–9
[48] Doyle M, Fuller T F and Newman J 1994 *Electrochim. Acta* **39** 2073–81
[49] Thomas K E, Sloop S E, Kerr J B and Newman J 2000 *J. Power Source* **89** 132–8
[50] Sun X G and Kerr J B 2006 *Macromolecules* **39** 362–72
[51] Blazejczyk A, Wieczorek W, Kovarsky R, Golodnitsky D, Peled E, Scanlon L G, Appetecchi G B and Scrosati B 2004 *J. Electrochem. Soc.* **151** 1762–6
[52] Byrne N, Efthimiadis J, Macfarlane D R and Forsyth M 2004 *J. Mater. Chem.* **14** 127–33
[53] Park C H, Sun Y–K and Kim D–W 2004 *Electrochim. Acta* **50** 375–8
[54] Feng S W, Shi D, Liu F, Zheng L, Nie J, Feng W, Huang X, Armand M and Zhou Z 2013 *Electrochim. Acta* **93** 254–63
[55] Ma Q *et al* 2016 *Angew. Chem. Int. Ed.* **55** 2521–5
[56] Shubha N, Zhu H, Forsyth M and Srinivasan M 2016 *Polymer* **99** 748–55
[57] Muthukumar M 2017 *Macromolecules* **50** 9528–60

[58] Chen G, Niu C, Chen Y, Shang W, Qu Y, Du Z, Zhao L, Liao X, Du J and Chen Y 2019 *Solid State Ion.* **341** 115048
[59] Kim J Y, Nagamani S, Liu L, Elghazaly A H, Solin N and Inganäs O 2020 *Biomacromolecules* **21** 1214–21
[60] Kim J Y 2018 *Macromolecules* **51** 9026–34
[61] Kim J Y 2019 *Macromolecules* **52** 4317–28
[62] Ratner M A 1987 *Polymer Electrolyte Reviews* ed J R MacCallum and C A Vincent (London: Elsevier Applied Science)
[63] Hiemenz P C 2007 Lodge T P *Polymer Chemistry* (USA, FL: CRC Press Taylor and Francis Group: Boca Raton)
[64] Cohen M H and Turnbull D 1959 *J. Chem. Phys.* **31** 1164
[65] Zundel G 1969 *Hydration and Intermolecular Intermolecular Interaction: Investigations With Polyelectrolyte Membranes* (New York: Acadamic Press) pp 36–124
[66] Yoshihara T, Tadokoro H and Murahashi S 1964 *J. Chem. Phys.* **41** 2902–11
[67] Idayu S, Halim A, Chan C H and Sim L H 2016 *Macromol. Symp.* **365** 95–103
[68] Sim L H, Gan S N, Chan C H and Yahya R 2010 *Spectrochim. Acta Part A Mol. Biomol. Spectrosc.* **76** 287–92
[69] Arnaud R, Benrabah D and Sanchez J 1996 *J. Phys. Chem.* **100** 10882–91
[70] Grondin J, Rey I, LasseÁgues J C and Servant L 1998 *Electrochim. Acta* **43** 1505–10
[71] Wen S J, Richardson T J, Ghantous D I, Streibel K A, Ross P N and Cairns E J 1996 *J. Electroanal. Chem.* **408** 113–8
[72] Bates F S 1991 *Science* **251** 898–905
[73] McNeil C R and Greenham N C 2009 *Adv. Mater.* **21** 3840–50
[74] Fanta G M, Jarka P, Szeluga U, Tanski T and Kim J Y 2020 *Polymers* **12** 1726
[75] Wunderlich B 1980 *Crystal Melting, Macromolecular Physics* vol 3 (New York: Academic Press)
[76] Yang S, Liu Z, Liu Y and Jiao Y 2015 *J. Mater. Sci.* **50** 1544–52
[77] Cullity B D and Stock S R 2001 *Elements of X-Ray Diffraction* (Upper Saddle River NJ: Prentice Hall)
[78] Kim J Y and Frisbie C D 2008 *J. Phys. Chem. C* **112** 17726–36
[79] Chabagno J M 1980 *Thesis* University of Grenoble
[80] Evans J, Vincent C A and Bruce P G 1987 *Polymer* **28** 2324–8
[81] Ma Q, Xia Y, Feng W, Nie J, Hu Y–S, Li H, Huang X, Chen L, Armand M and Zhou Z 2016 *RSC Adv.* **6** 32454–61
[82] Conway B E 1998 *Electrochemical Supercapacitors: Scientific Fundamentals and Technological Applications* (New York: Kluwer Academic/Plenum Publishers)